Dynamics of groundwater recharge and seepage over the Canadian landscape during the Wisconsinian glaciation

J.-M. Lemieux,[1] E. A. Sudicky,[1] W. R. Peltier,[2] and L. Tarasov[3]

[1] Pleistocene glaciations and their associated dramatic climatic conditions are suspected to have had a large impact on the groundwater flow system over the entire North American continent. Because of the myriad of complex flow-related processes involved during a glaciation period, numerical models have become powerful tools for examining groundwater flow system evolution in this context. In this study, a series of key processes pertaining to coupled groundwater flow and glaciation modeling, such as density-dependent (i.e., brine) flow, hydromechanical loading, subglacial infiltration, isostasy, and permafrost development, are included in the numerical model HydroGeoSphere to simulate groundwater flow over the Canadian landscape during the Wisconsinian glaciation (~ -120 ka to present). The primary objective is to demonstrate the immense impact of glacial advances and retreats during the Wisconsinian glaciation on the dynamical evolution of groundwater flow systems over the Canadian landscape, including surface-subsurface water exchanges (i.e., recharge and discharge fluxes) in both the subglacial and the periglacial environments. It is shown that much of the infiltration of subglacial meltwater occurs during ice sheet progression and that during ice sheet regression, groundwater mainly exfiltrates on the surface, in both the subglacial and periglacial environments. The average infiltration/exfiltration fluxes range between 0 and 12 mm/a. Using mixed, ice sheet thickness–dependent boundary conditions for the subglacial environment, it was estimated that $15-70\%$ of the meltwater infiltrated into the subsurface as recharge, with an average of 43%. Considering the volume of meltwater that was generated subsequent to the last glacial maximum, these recharge rates, which are related to the bedrock type and elastic properties, are historically significant and therefore played an immense role in the evolution of groundwater flow system evolution over the Canadian landmass over the last 120 ka. Finally, it is shown that the permafrost extent plays a key role in the distribution of surface-subsurface interaction because the presence of permafrost acts as a barrier for groundwater flow.

1. Introduction

[2] During the Quaternary period, cyclic glaciations have occurred over a global scale as the result of a climatic variability that affected the Earth's atmospheric, oceanic and glacial systems. These glaciation periods were characterized by the growth of immense ice sheets covering North America and Europe over a period on the order of about 100 ka followed by fairly rapid deglaciation periods.

[1] Department of Earth and Environmental Sciences, University of Waterloo, Waterloo, Ontario, Canada.
[2] Department of Physics, University of Toronto, Toronto, Ontario, Canada.
[3] Department of Physics and Physical Oceanography, Memorial University, St. John's, Newfoundland and Labrador, Canada.

[3] It is well documented that severe global-scale environmental perturbations accompanied these glacial periods. For example, during the last glacial maximum (LGM), at about -21 ka, the Canadian landscape was almost entirely covered with ice. The Laurentide ice sheet, the largest of the three North American ice sheet complexes, reached a maximum thickness of about 4.5 km and the force exerted by its weight on the Earth's crust was sufficient to cause a depression of the surface up to about 1 km and thus a dramatic overpressurization of pore water fluids. Extreme atmospheric conditions, accompanying the progression of the ice, caused the freezing of soils and rocks at low latitudes to a depth of up to 1 km into the subsurface. Mean sea level fluctuated by several tens of meters and reached a level of -120 m relative to present at LGM.

[4] Although the ice sheets grow during a glaciation period, the friction at the ice-bed interface as well as the

vertical deep-seated geothermal heat flux tends to produce a large amount of subglacial meltwater. This meltwater was, until recently, considered to be drained only as channel and sheet flow at the ice-bed interface, thus being conceptualized as a source of rapid surface water runoff. Recently, several studies have indicated that significant subglacial meltwater can infiltrate into the subsurface under the ambient ice sheet pressure and therefore becomes stored in the groundwater flow system [e.g., *Clark et al.*, 2000; *Douglas et al.*, 2000; *Grasby et al.*, 2000; *Ferguson et al.*, 2007; *Person et al.*, 2007]. Because of the small pore spaces within the underlying rocks, a relatively small quantity of recharge into the subsurface can considerably raise pore pressures and therefore modifies the groundwater flow field.

[5] Because many processes affect groundwater flow system evolution during a glaciation period and because these processes are typically strongly coupled, numerical models have become powerful tools to study the impact of glaciation on groundwater flow dynamics over large time frames. In the recent literature, several authors have presented results from numerical modeling studies on the affects of glaciation on groundwater flow [e.g., *Boulton et al.*, 1995; *Piotrowski*, 1997; *Person et al.*, 2003]. The approaches taken are diverse, but all large-scale studies have ignored important factors known to influence groundwater flow pattern. Moreover, most of these studies considered either two-dimensional (2-D) cross-sectional or 2-D areal flow models, when it is known that 3-D effects are important at regional or continental scales, and many were performed by assuming a series of steady state time slices. A glaciation is, however, a highly transient event even if groundwater pressures at depth evolve relatively slowly.

[6] In this study, published techniques to model the coupling between glaciations and groundwater flow will be briefly reviewed. A list of the important processes related to glaciation that can affect groundwater flow system evolution will be drawn and appropriate means to include them in a numerical model will be introduced. The resulting numerical model will then be used to simulate 3-D continental-scale groundwater flow over the Canadian landscape during the Wisconsinian glaciation and salient results pertaining to surface-subsurface water interaction will be presented. The groundwater flow model is driven by a surface glacial systems model that provides the boundary conditions.

2. Ice and Climate Model

[7] The coupling of climate models to groundwater flow models is usually performed by an asynchronous forcing of the groundwater flow model with the results of a climate model, usually a global circulation model. The approach used in this study is similar, but the complexity arising from the glacial component of the climate model raises the need to include a more complex set of boundary conditions not commonly used in conventional groundwater flow modeling studies. We include other important factors such as the influence of permafrost development/thawing, changing topography due to isostasy, sea level change on coastal margins due to ice sheet formation/thawing and the presence of high-salinity paleobrines at depth in the continental interior.

[8] The inferred ice and climate chronologies during the Wisconsinian glaciation presented here are derived from the Memorial University of Newfoundland/University of Toronto Glacial Systems Model (GSM). The GSM was executed over the past 120 ka on a $1.0°$ longitude by $0.5°$ latitude grid resolution in order to produce a data set for surface elevation, ice sheet thickness, relative sea level and subglacial melt rate. A detailed description of the model and its calibration is given in Appendix A.

3. Governing Equations

[9] A well-documented geochemical feature of Canadian Shield groundwaters is the occurrence of brines of a relatively uniform composition over the entire Shield [*Frape and Fritz*, 1987]. Brines occurrence is also documented in the sedimentary basins of the northern United States and southern Ontario [*Siegel*, 1989; *Dollar et al.*, 1991; *McIntosh et al.*, 2002] and in the Western Sedimentary Basin [*Spencer*, 1987]. The major ions composing the brines are Ca-Na-Cl and their concentrations increase with depth. Because of this characteristic, a density-dependent formulation of groundwater flow is essential. Along with the effect of density on groundwater flow, the surface loading by glacial ice produces a mechanical deformation of the Earth crust which increases pore pressure. *Wang* [2000] and *Neuzil* [2003] assert that the assumption of purely vertical strain is a reasonable assumption in two- and three-dimensional flow regimes, resulting in small errors due to laterally extensive overburden changes. The assumptions of purely vertical strain and constant vertical stress are therefore used here to describe transient groundwater flow. Use of this assumption to handle hydromechanical deformation, and inclusion of density-dependent groundwater flow, can be described by the following groundwater flow equation:

$$\frac{\partial}{\partial x_i}\left(K_{ij}\frac{\mu_0}{\mu}\left(\frac{\partial h^*}{\partial x_j}+\rho_r\frac{\partial z}{\partial x_j}\right)\right)$$
$$=S_s\frac{\partial h^*}{\partial t}-S_s\zeta\frac{1}{\rho g}\frac{\partial \sigma_{zz}}{\partial t}, \quad i,j=1,2,3 \tag{1}$$

where K_{ij} is the hydraulic conductivity tensor [L T^{-1}], S_s is specific storage [L^{-1}], ζ is the one-dimensional loading efficiency [dimensionless], ρ is the density of water [M L^{-3}], g is the gravitational acceleration [L T^{-2}], h^* is the freshwater head [L], ρ_r is the relative density [M L^{-3}], μ_0 is the reference viscosity [M L^{-1} T^{-1}], $\mu(T,c)$ is water viscosity [M L^{-1} T^{-1}], ρ_0 is the reference density [M L^{-3}] and σ_{zz} is the vertical stress [M T^{-2} L^{-1}] caused by the ice weight.

[10] The one-dimensional loading efficiency, ζ, is the ratio of surface loading that is transferred to the fluid and can be computed from the elastic properties of rock. Although it is possible to compute the loading efficiency coefficient using data for the compressibility of the porous medium and water, and Poisson's ratio, the paucity of representative data introduces considerable uncertainty. A value for loading efficiency is often chosen between zero and one and can be evaluated with a sensitivity analysis.
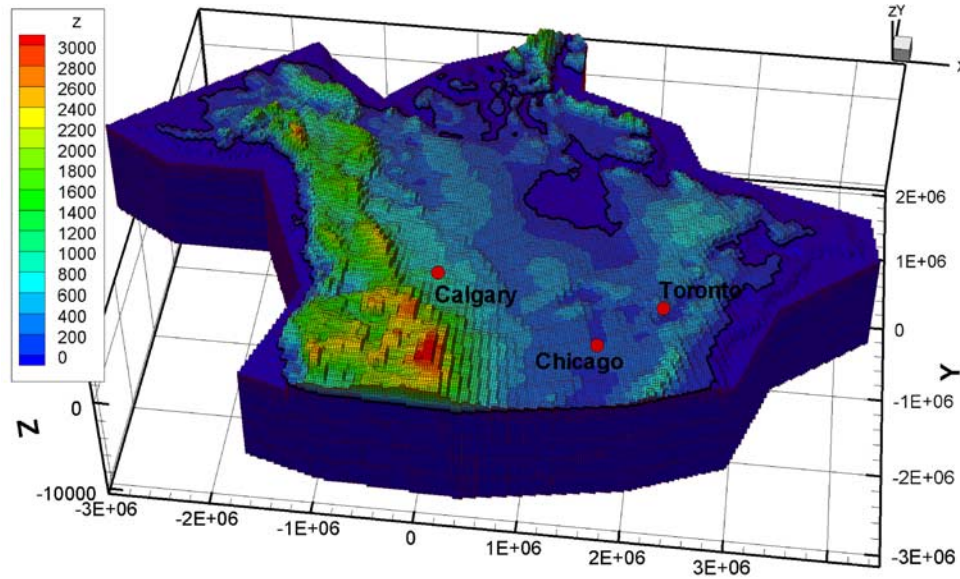
Figure 1. Three-dimensional mesh used for groundwater flow simulations. The finite element mesh contains 404,960 brick elements and 452,034 nodes. The *xyz* coordinates are in meters projected with the Albers equal-area map projection. Vertical exaggeration is ×150.

[11] The solute transport continuity equation, including a first-order source term for brine generation, is given by

$$\frac{\partial}{\partial x_i}\left(\phi D_{ij}\frac{\partial c}{\partial x_j} - q_i c\right) + \Gamma_{1st} = \frac{\partial(\phi c)}{\partial t}, \quad i, j = 1, 2, 3 \quad (2)$$

where ϕ is porosity [dimensionless], D_{ij} is the dispersivity tensor [$L^2\ T^{-1}$] and c is concentration [$M\ L^{-3}$]. In order to represent brine formation, a process that depends on the difference of concentration between total dissolved solids (TDS) in the fluid and a potential maximum concentration generated by rock weathering, leaching of saline fluid inclusions or other processes is used. A first-order source term [$M\ T^{-1}\ L^{-3}$], Γ_{1st}, is defined as [*Provost et al.*, 1998]

$$\Gamma_{1st} = k_{mt}(c_{max} - c) \quad (3)$$

where k_{mt} is a mass transfer coefficient rate [T^{-1}] describing rock-water mass interactions and c_{max} is the maximum allowable fluid concentration [$M\ L^{-3}$]. The maximum allowable fluid concentration, c_{max}, could represent the saturation concentration of TDS in the case of rock weathering or the concentration of TDS in fluid inclusion, in the case of leaching [*Provost et al.*, 1998].

[12] The concentration is linked to the fluid density with the linear relationship $\rho_r = (\rho_{max}/\rho_0 - 1)\ (c/c_{max})$. These coupled equations are solved using the control volume finite element numerical model HydroGeoSphere [*Therrien et al.*, 2006].

4. Computational Domain

[13] The numerical model described above is used to simulate groundwater flow and solute transport during the Wisconsinian glaciation over the Canadian landscape. The finite element mesh used encompasses all of Canadian landscape as well as the northern United States and contains 404,960 brick elements and 452,034 nodes (Figure 1). Along the z axis, 10 layers are used over depth between the temporally changing surface elevation and an elevation of -10 km below present-day mean sea level. The modelled region covers a large region of the Earth's surface and because HydroGeoSphere does not support spherical coordinates, a projection to a Cartesian coordinate system was used. The Albers equal-area conical projection was utilized because it minimizes distortion and preserves area. The lateral dimensions of the brick elements are 25 km and their vertical thicknesses vary between 50 m near the surface to 1000 m at depth.

[14] The bedrock geology was simplified into four major facies (Figure 2). The first facies represents the Canadian Shield, the second facies includes the sedimentary basins, and the third facies is referred to as the orogen and represents the Appalachian, Rockies, and Innuitian orogenic belts. The last facies is the oceanic crust that extends around the North American continent. The hydraulic properties of the different facies are given in Table 1. The hydraulic properties were obtained from a detailed review of the literature [*Lemieux*, 2006]. Although the surface hydraulic conductivity of the Canadian Shield might seem high, its value is decreasing rapidly with depth as discussed below. Unconsolidated surficial sediments are not represented explicitly in the current simulations; their representation is a topic of future efforts. Instead, their hydraulic properties was set to the underlying rock type. Given that the thickest unconsolidated deposits are over sedimentary rocks and that thin unconsolidated sediments covers the Canadian Shield, and given the areal scale and depth extent of the present domain, it is believed that their explicit inclusion in the model will not dramatically alter the groundwater flow system patterns at large depths, although this aspect requires
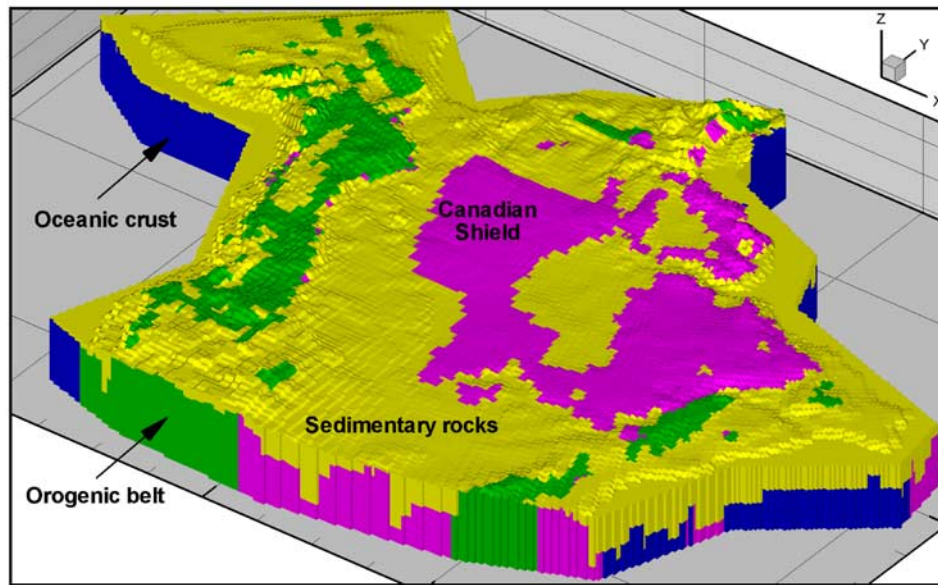
Figure 2. Simplified bedrock geology facies used in the numerical model shown for the entire simulation domain. Colors are as follows: pink, Canadian Shield; dark green, orogenic belts; dark blue, oceanic crust; and yellow, sedimentary rocks. The figure is constructed from *Bassin et al.* [2000] and *Wheeler et al.* [1997].

further exploration. Moreover, the sediment distribution is expected to greatly evolve during a glacial period and details concerning their spatiotemporal evolution over the model domain are presently unavailable.

[15] Because hydraulic conductivity is expected to decrease with depth because of increasing effective stresses and temperature-dependent diagenetic and metamorphic processes [*Ingebritsen and Sanford*, 1998], surface hydraulic conductivity values are reduced with depth on a logarithmic scheme based on published data from the tests conducted in a number of deep boreholes and underground workings [*Ingebritsen and Sanford*, 1998]. While the input solute (brine) dispersion parameters shown in Table 1 are exceedingly large (i.e., the scale of the grid block discretization), a preliminary analysis indicated that the subsurface brine distribution is not overly sensitive to these parameters because the brines cover vast areal extents at depth over the continent.

[16] The simulation spans over the last 120 ka with a time discretization of 100 years. The initial conditions were

obtained from a pseudo steady state simulation, i.e., a transient simulation run until near steady state conditions, using the climatic conditions of the last interglacial. Subsequently, the ice load–related boundary conditions, topography (from isostasy), surface water load, subglacial meltwater rates, and permafrost thicknesses were obtained from the GSM and applied to the model every 1 ka using the methodology described in the next section. Although the GSM time step is 12.5 years or less, the major trends of the surface boundary conditions could easily be captured with 1 ka time step, which considerably reduced the amount of memory needed to store the boundary conditions and allowed the use of larger time step for faster simulation time.

5. Hydraulic Conditions During a Glacial Cycle

[17] During a glacial cycle, the surface boundary conditions can be quite different than at present time and evolve from temperate to polar conditions. During the last inter-

Table 1. Bedrock Hydraulic Properties by Facies[a]

Parameter	Facies			
	Sedimentary	Shield	Orogen	Oceanic Crust
K, m/a	60.0	30.0	3.0	0.1
Specific storage, S_s, m^{-1}	5.0×10^{-5}	3.0×10^{-6}	1.0×10^{-5}	1.0×10^{-5}
Porosity, ϕ	0.2	0.001	0.05	0.01
Loading efficiency, ζ	0.2	0.2	0.2	0.2
Longitudinal dispersivity, α_L, m	50 000	50 000	50 000	50 000
Transverse dispersivity, α_T, m	1 000	1 000	1 000	1 000
Transverse vertical dispersivity, α_V, m	1 000	1 000	1 000	1 000
Rock-water mass transfer constant, k_{mt}, a^{-1}	2.3×10^{-7}	2.3×10^{-8}	2.3×10^{-8}	2.3×10^{-9}

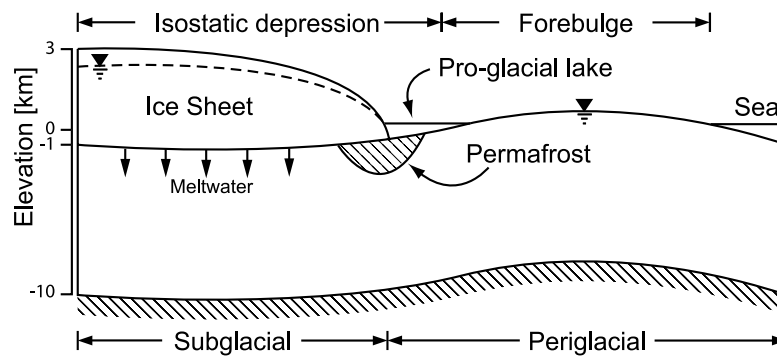[a]The hydraulic conductivity is isotropic and is given for the surface elements.

Figure 3. Cross section along an ice flow line showing hydraulic conditions during a glacial cycle. Extent of the subglacial and periglacial environments is also shown.

glacial, ~120 ka ago, the climatic conditions were quite similar to present and therefore the continental hydrogeology is surmised to be similar to present conditions. Figure 3 is a simplified cross section that illustrates the boundary conditions that will be described in this section and used to couple the results from the GSM with the subsurface flow model.

[18] As the ice sheet grows, its weight will cause the Earth's crust to deform. The deformation of the crust by the ice sheet is such that the Earth's surface elevation will be depressed underneath the ice sheet and raised beyond its margins. The elevations of the grid nodes in each vertical column of the model beneath the ice sheet are adjusted uniformly because the entire crust is depressed uniformly according to the physically based GSM crustal deformation predictions. Because the surface elevation changes from one time step to the next are relatively small, it is believed that this uniform vertical coordinate adjustment of each vertical column of nodes will not produce significant fluid mass balance errors. On the other hand, we expect that the temporally and areally changing topographic elevation will have a significant transient impact on groundwater flow patterns.

5.1. Periglacial Conditions

[19] When the ice sheet begins to grow and flows from high latitudes to lower latitudes, it also brings with it lower temperatures and the permafrost zone migrates southward with the ice sheet. In regions where permafrost forms, the relative permeability of the subsurface materials is greatly reduced. These regions are believed to exist at the ice sheet margins and under the center of ice domes [e.g., *Hughes*, 1998; *Boulton et al.*, 1996; *Boulton and de Marsily*, 1997; *King-Clayton et al.*, 1995]. Permafrost forms because of very low temperatures and propagates downward to a depth of as much as 1000 m. While an ice sheet covers frozen ground, the temperature of the subsurface will slowly increase up to the pressure melting point because the ice sheet acts as an insulating blanket from the extremely low surface temperatures. The permafrost therefore migrates along the periphery of the ice sheet margins.

[20] The permeability of soils and rocks affected by permafrost is greatly reduced [*Burt and Williams*, 1976] but there is no consensus on the permeability reduction because of a paucity of data [*Boulton and de Marsily*, 1997].

The main effect of extensive permafrost is that it prevents surface water from recharging groundwater and conversely from allowing groundwater to discharge to the surficial regime [*McEwen and de Marsily*, 1991]. Permafrost does not develop instantaneously; the freezing of water in the soil is instead a transient process. As water in the pores freezes, the permeability of the subsurface material to water is reduced. In the numerical model, the hydraulic conductivity of elements affected by permafrost is simply allowed to vary between its frozen and unfrozen states. For the frozen state, a low hydraulic conductivity is specified (i.e., a 6 order of magnitude reduction) and, for the unfrozen state, the medium's default hydraulic conductivity value is used. Between these states, the permeability values are interpolated linearly between time steps so that they are progressively reduced or increased depending on the thermal regime. Time slices of 1000 years were selected to specify frozen/unfrozen states.

[21] After the glacial maximum, the ice sheet begins to melt and retreats northward fairly rapidly. On the land surface, large proglacial lakes form at the ice margin in the isostatic depressions. The depth of the depressions evolves as the Earth's crust recovers to its initial state. Several large proglacial lakes formed during the last deglaciation period and their configuration, depth and extent was a result of the interactions among the location of the ice margin, the topography of the newly deglaciated surface, the elevation of the active outlet, and differential isostatic rebound [*Teller*, 1987].

[22] For periglacial conditions, an assumption that the water table elevation equals to the topographic surface is made. In Canada, the water table is rarely deeper than a few meters to tens of meters and it is believed that it will remain the case during a glaciation period. The water table is therefore specified to equal the surface elevation for all the nodes not covered by ice. At some point, during the deglaciation period, the water table is higher than the surface because of the filling of surface depressions by meltwater and proglacial lakes, such as the immense Lake Agassiz (−12 ka to −8 ka). As such, grid nodes covered by paleolakes predicted by the GSM model [*Tarasov and Peltier*, 2005] are assigned a subsurface head values equal to the surface elevation plus the depth of the surface water body, all of which are treated as transient. During some periods of time, the ocean level had risen to levels higher

than the previous shoreline such that the land surface was covered by seawater. The nodes covered by the sea were therefore assigned a hydraulic head equal to the sea level at that time, which is given by the predicted relative sea level data.

5.2. Subglacial Hydraulic Conditions

[23] When the ice sheet grows to cover the frozen ground beyond its margins, the subglacial temperature below the advancing ice sheet warms up to the melting point because the Earth's surface is isolated from the cold atmospheric conditions and because the vertical geothermal gradient brings the necessary energy from the Earth's core. The pressure of the ice sheet also contributes to the lowering of the melting point, at a rate of 0.87° Celsius per km of ice. Away from the center of ice domes, ice deformation heating and basal friction will further contribute to the production of subglacial meltwater. This meltwater is under ice sheet pressure and, when the permeability of the subglacial sediments or bedrock is sufficient, the meltwater is driven into the subsurface. In the case of unconsolidated sediments, the effective pressure may become very small and the strength of the sediments is reduced [*van Weert et al.*, 1997] and the erosion and deformation of sediments is favored [*Shoemaker*, 1986].

[24] The subglacial meltwater that infiltrates into the subsurface will flow from high hydraulic head zones (i.e., under the ice sheet) to lower head zones which can either be subglacial regions where there is no melting or to distal areas beyond the limits of the ice sheet. Groundwater flow lines therefore mimic in an ancillary way the nature of ice sheet flow lines. At the tip of the ice sheet, large subsurface hydraulic gradients form over short distances, but the permeability is greatly reduced by the presence of the permafrost. These conditions are likely to lead to hydrofracturing in sediments and rocks at the ice sheet margin [*Boulton et al.*, 1996]. Laterally beyond the permafrost zone, through local gaps in the discontinuous permafrost, strong upward groundwater flow is likely to occur that will lead to sediment liquefaction, sediment dyke formation and sediment expulsion structures [*Boulton et al.*, 1996]. The subglacial meltwater that does not infiltrate into the subsurface will flow along the ground-ice interface. This may involve various morphologies of conduits incised into the ice or ground, sheet flow at the interface, and/or diffusive flow through the surface sediment, depending on the nature of the substrate, water pressure and flux, bed geometry, and sliding speed of the ice [*Paterson*, 1994].

[25] The proportion of subglacial meltwater that infiltrated and was stored in the subsurface is uncertain and is a question of much debate in the literature because of its relevance to many issues regarding current freshwater resources management, sustainability, and anthropogenic activities. There are several approaches that have been used to calculate recharge rates during glaciations, but they do not seem to deliver plausible results. *Breemer et al.* [2002], for example, specify a constant flux equal to the subglacial meltwater rate and obtain unrealistically high subsurface hydraulic heads in their model of the Michigan Lobe. They also examined a case having a high-permeability layer between the bedrock and the ice sheet. Only with the inclusion of a thin highly permeable layer at the ice/bedrock interface, represented

numerically by a highly transmissive fracture-type layer, could realistic subsurface heads be computed by the model. The permeability of such a layer, and the spatiotemporal patterns of its permeability, becomes an issue for which little data exits. *McIntosh and Walter* [2005] and *Forsberg* [1996] use a prescribed subsurface potentiometric surface equal to the ice sheet thickness, expressed in terms of the equivalent freshwater head. This approach implies the assumption that the subglacial pressure never declines below the equivalent ice sheet load, which commonly cannot be demonstrated. *Piotrowski* [1997] also used a prescribed subsurface potentiometric surface in his groundwater model at locations where the ice sheet covers the bedrock, but with the difference that it was inferred from paleopore water pressures estimated from the stress characteristics of the fine-grained sediments overridden by the ice sheet [*Piotrowski and Kraus*, 1997]. According to these proxy estimates, the potentiometric surface was on average equal to 72% of the ice thickness. This approach seems to lead to realistic infiltration rates, but is restricted to the relatively small regions under study for which paleopore water pressure data are available. Another approach was used by *Svensson* [1999], *Boulton et al.* [2001], and *Jaquet and Siegel* [2003] in which a specified meltwater rate is applied subglacially with the explicit inclusion of discrete subglacial tunnels (eskers) that will lower the water table because of their high hydraulic conductivity. An arbitrary adjustment of the hydraulic conductivity of these tunnels can be made to achieve subglacial pressures slightly lower than the equivalent pressures induced by the ice sheet thickness to yield realistic infiltration rates. The major drawback of this approach is that the position, geometry and interconnectivity of the tunnels, and their hydraulic properties, must be known a priori; without this knowledge, it is clear that a stochastic, but geologically constrained, probabilistic approach is needed. Finally, a detailed 2-D subglacial hydrology model that couples glacier surface runoff, englacial water storage and transport, subglacial drainage, and subsurface groundwater flow was presented by *Flowers and Clarke* [2002a, 2002b] but is limited to the catchment scale.

[26] The modeling approaches mentioned above to force glaciation model output to groundwater flow models are based on a number of assumptions or process-related simplifications, especially when applied to the scale of the entire Canadian landmass. Here, we use a mix of time-dependant boundary conditions that are more natural and more constrained than other studies. The manner in which subglacial meltwater enters the subsurface in the model is prescribed by a groundwater recharge flux that is dynamically constrained by the ice sheet thickness from one time step to the next. A specified groundwater recharge flux that is equal to the predicted subglacial meltwater rate is applied to the subsurface only as long as the hydraulic head at the glacier's bed is lower than the ice equivalent freshwater head; otherwise the equivalent ice sheet head at any node in the computational grid and its difference with the groundwater head at the same location is used to control the subsurface subglacial infiltration; the remainder is treated as direct overland runoff. The reasoning behind this treatment is that if the subsurface hydraulic head becomes higher than the equivalent ice sheet load, the ice sheet would float and become unstable. The solution is analyzed after each

time step and if any of the surficial grid nodes have a head higher than the equivalent ice load, the time step is started again with a head specified to the ice load for those nodes. This approach allows the computation of the fraction of the meltwater that can naturally infiltrate into the subsurface with the remainder assumed to participate in the surface flow regime. A more formal description of the numerical model is given by *Lemieux* [2006].

6. Results

[27] Although the simulation presented here embodies a fully 3-D subsurface head distribution along with the coupled evolution of brine concentrations over the Canadian landscape over the last ~120 ka, this paper will only present results related to the calculated surface-subsurface water flow interactions over the subglacial and periglacial environments. As discussed above, our current knowledge of the paleoglacial-subglacial environments occurring at a variety of scales remains uncertain because of the complexity of the processes involved. Nevertheless, the model has been calibrated with total dissolved solids measurements from the Canadian Shield, Western Sedimentary Basin and the Michigan Basin [*Lemieux*, 2006].

[28] A base case scenario is first presented with the hydraulic properties discussed in the previous sections. A sensitivity analysis of key parameters such as loading efficiency and permafrost hydraulic conductivity is then performed to capture their influence on the recharge and discharge patterns across the land surface.

6.1. Base Case Scenario

[29] Figure 4 shows the calculated surface-subsurface water exchange fluxes in the subglacial environment during the glaciation period. Along with the total flux crossing the ground surface, the volumetric infiltration (positive) and exfiltration (negative) fluxes are also shown. The volumetric fluxes shown in Figure 4a are large because they are integrated values over the entire subglacial environment. When expressed as a flux (Figure 4b), the infiltration ranges between 0 and 6 mm/a with an average of about 2.5 mm/a. The exfiltration (i.e., groundwater discharge) flux can reach values up to about 12 mm/a with an average of 2.0 mm/a. The exfiltrating fluxes reach higher values than infiltration because the area of the exfiltrating portion of the subglacial environment is much smaller than the infiltration portion.

[30] The GSM-predicted total surface area of the glacial ice is shown in Figure 4a and can be used as an indicator of ice sheet progression or regression; an increase in the total surface area indicates ice sheet progression over the land surface and a decrease in surface area indicates that the ice sheet is regressing. It can be seen from Figure 4a that there were three major glacial advances/regressions during the Wisconsinian glaciation and that maxima in the ice volumes occurred at about −105, −60 and −21 ka (GM1, GM2 and GM3 in Figure 4a) which occurs as a consequence of the Earth obliquity orbital cycle around the sun. It can be seen that, in the subglacial environment, most of the infiltration of the meltwater into the subsurface occurs when the ice sheet is growing. Conversely, groundwater mainly exfiltrates during ice sheet regression. Because of the high pressures at the bed of the ice sheet, meltwater is forced downward into the subsurface during ice sheet advance and, when the ice sheet is regressing, the pressure in the subsurface becomes higher than the basal meltwater pressure and groundwater exfiltrates.

[31] The relationship between the exchange flux regime and the ice sheet progression can also be observed in Figures 5a, 5c, and 5e where the spatial pattern of the surface-subsurface water exchange flux is shown over the entire simulation domain for three time slices. The slices are chosen to capture the portion during ice sheet during progression (−30 ka), at the end of the ice sheet progression (at LGM, −20 ka) and during ice sheet regression (−14 ka). Again, it can be seen that infiltration dominates during ice sheet progression while exfiltration dominates during ice sheet regression, although both regimes are always active at different locations.

[32] The mixed boundary condition used at the subglacial faces of the upper elements in the mesh allows computation of the ratio of the total meltwater that is infiltrating the subsurface to the total meltwater production. The integration of the infiltration ratio over the entire subglacial environment shows that the infiltration ratio oscillates between 15% and 100%, with an average of about 43%, that was obtained by integrating the infiltration ratio curve (Figure 6). This indicates that a large fraction of the meltwater actually enters the subsurface. The infiltration ratio reaches its lowest value (15%) during the last glacial advance, which is also the period that produced the largest amount of meltwater. It can be seen that the infiltration diminishes shortly after the initiation of the three glacial advances GM1, GM2 and GM3.

[33] Throughout the glacial cycle, only a fraction of the subglacial meltwater infiltrates into the subsurface, which means there is an excess of meltwater. Because the rock permeability is not sufficient to drain all of the meltwater, subglacial pressures will buildup until the pressure reaches the ice load pressure. At this point, the pressure will remain at the ice load pressure until the predicted meltwater production diminishes. During this period, the excess meltwater is assumed to drain out of the model through a series of subglacial conduits. The infiltration process at the ice weight pressure then becomes a function of the ice thickness and is no longer a function of the meltwater production. Therefore the ice sheet thickness plays a key role in the infiltration process.

[34] The infiltration rate into the subsurface is expected to be different for sedimentary rocks than for Shield rocks because the hydraulic conductivity of the sedimentary rocks is higher. The calculation of the infiltration rate for both type of rocks for the whole glacial cycle is shown in Figure 7. It can be seen that the infiltration rates are higher for the sedimentary rocks that for the Shield rocks, and that the difference is even larger during the glacial advances. The difference between the subglacial infiltration in the Canadian Shield and sedimentary basins was also inferred by *Grasby and Chen* [2005] with the observation of the esker distribution across the Canadian landscape. They found that the eskers, which form in poor draining conditions, were distributed mainly in the Canadian Shield, suggesting that subglacial meltwater experienced limited infiltration, as opposed to the sedimentary basin, where the structures were not observed.
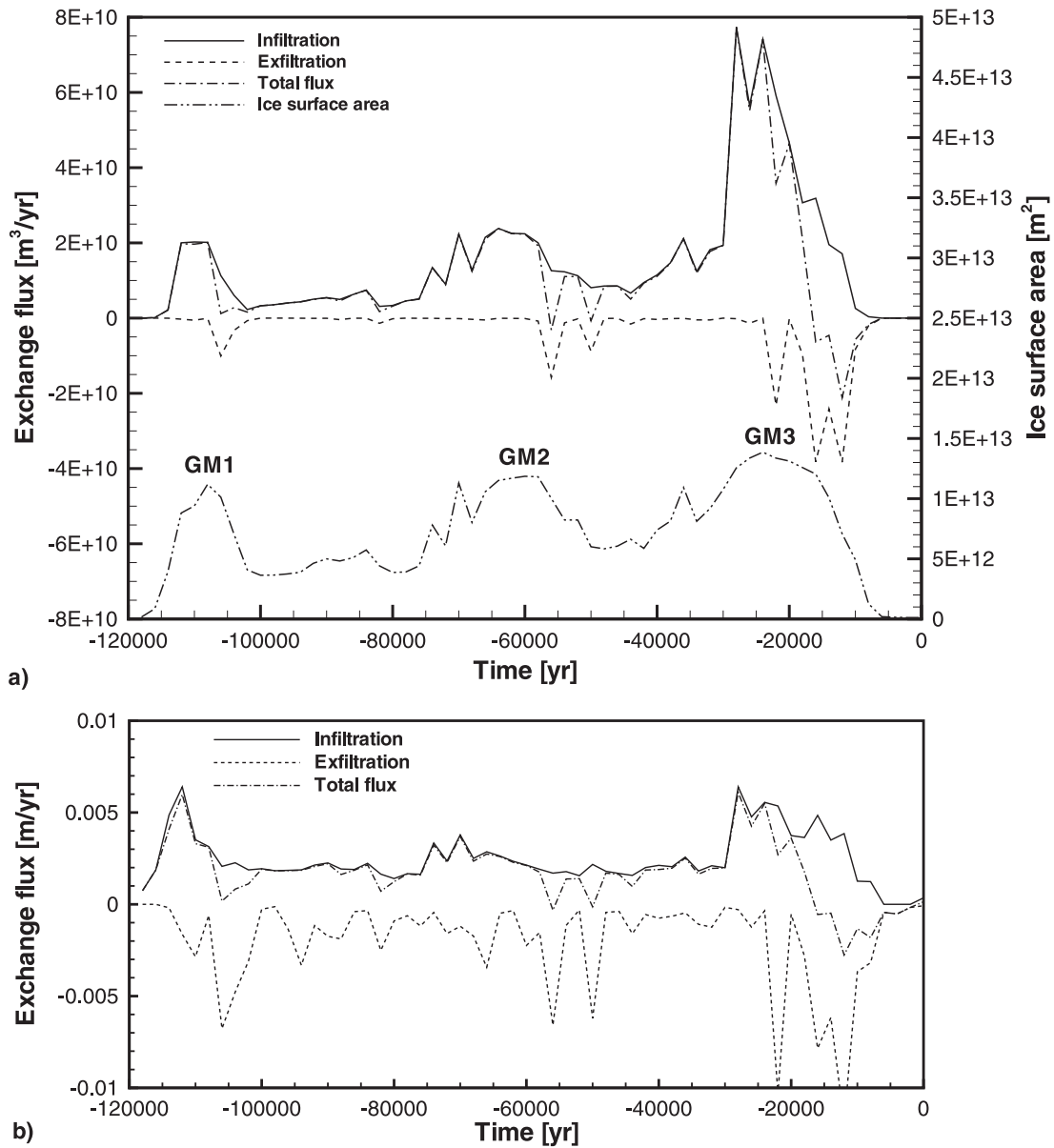
Figure 4. Subglacial exchange flux during the glacial cycle. (a) Volumetric exchange flux in m³/a. The curves represent the integration of the flux over the entire subglacial environment. The ice sheet surface area is also shown with the timing of the glacial maxima GM1, GM2, and GM3. (b) Exchange flux in m/a. Note: Positive values are for infiltration flux, and negative values are for exfiltration flux.

[35] The surface-subsurface water interaction in the periglacial environment has some similarity to that in the subglacial environment; most of the exchange flux is dominated by exfiltration during ice sheet regression, as shown by the volumetric exchange fluxes presented in Figure 8a and illustrated in a two-dimensional map of the exchange flux during ice sheet regression (Figure 8b). This situation occurs because the retreat of the ice sheet reveals a fringe of subsurface materials that are under ice sheet pressure and experiencing meltwater infiltration. Similar to the subglacial environment, when the ice sheet is retreating, the hydraulic gradient is reversed and groundwater exfiltrates across land surface or into large proglacial lakes. At the ice margin, a large hydraulic gradient develops between the ice-covered region and the periglacial zone.

In absence of permafrost or for a thin frozen depth, this large hydraulic gradient will increase the exfiltration flux at the margin.

[36] The periglacial infiltration flux is quite low over the time span of the simulation (Figure 8a) and represents infiltration at ice-free high-elevation regions over the Canadian landscape. After the last glacial maximum, the infiltration flux in the periglacial environment rises suddenly. Rapid filling of proglacial lakes may explain this infiltration augmentation. Increasing hydraulic heads due to the development of the proglacial lakes in regions of low topographic elevation have a large impact on the hydraulic gradient.

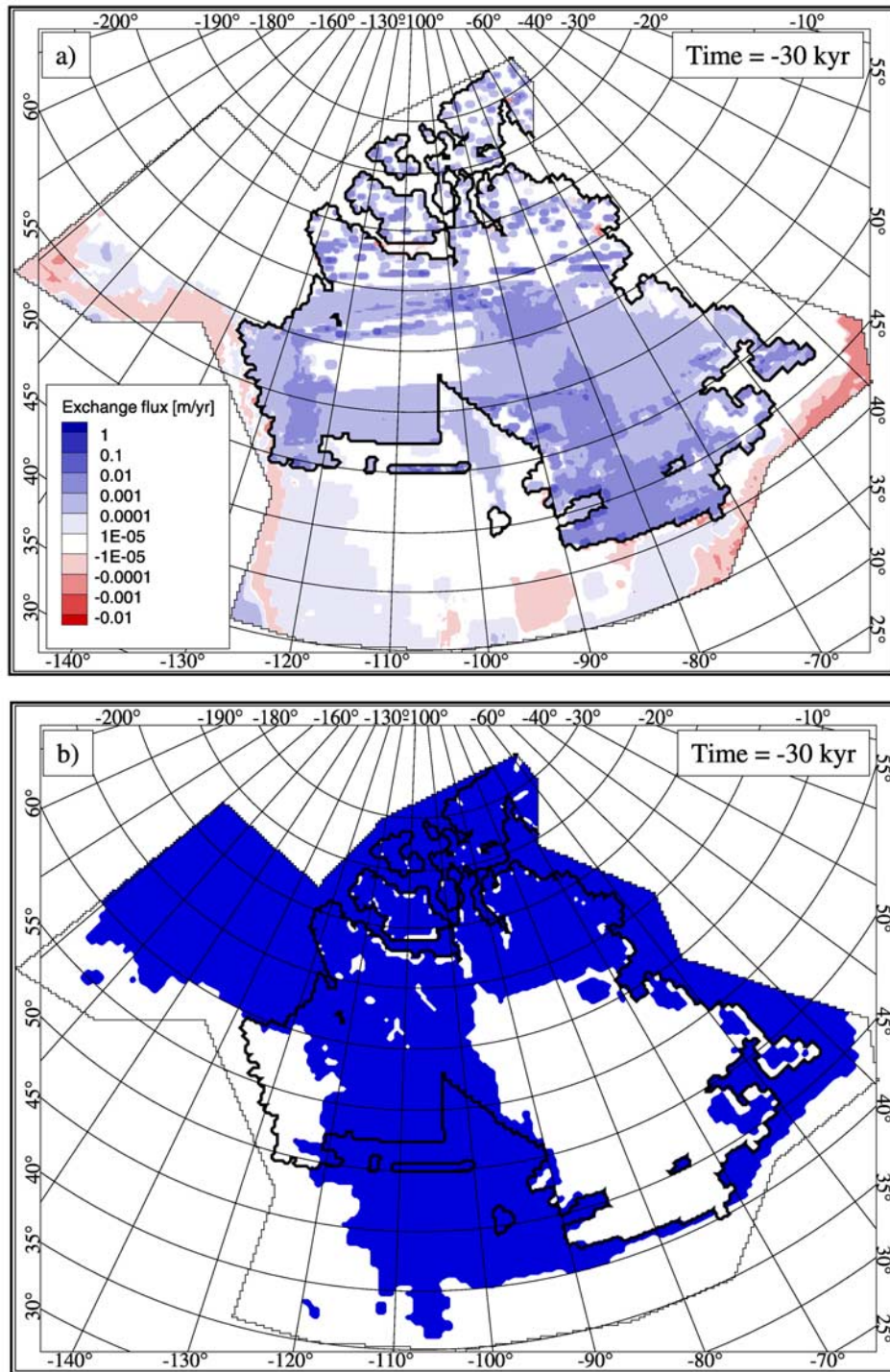[37] It can be seen from Figure 8b that the periglacial exchange flux is much lower than the subglacial exchange

Figure 5. Simulated surface-subsurface water exchange flux and surface permafrost distribution at (a, b) −30, (c, d) −20, and (e, f) −14 ka. The surface permafrost distribution is represented in blue, indicating the surface finite elements affected by permafrost. The black line indicates the ice sheet limits.

flux (Figure 8b); its magnitude is about three orders lower than that in the subglacial environment. During an interglacial period, the infiltration flux is about 0.03 mm/a which is of the same order of magnitude as the infiltration flux in the periglacial environment. Except for the large exfiltration fluxes, the periglacial exchange fluxes during the glacial cycle are similar to those during the interglacial and the values are quite low. The infiltration into the subsurface during a glacial cycle can be three orders of magnitude higher than during interglacial periods, such as the current one.

[38] The rates of groundwater recharge, over the Canadian Shield are not well documented. A compilation from *Heath*
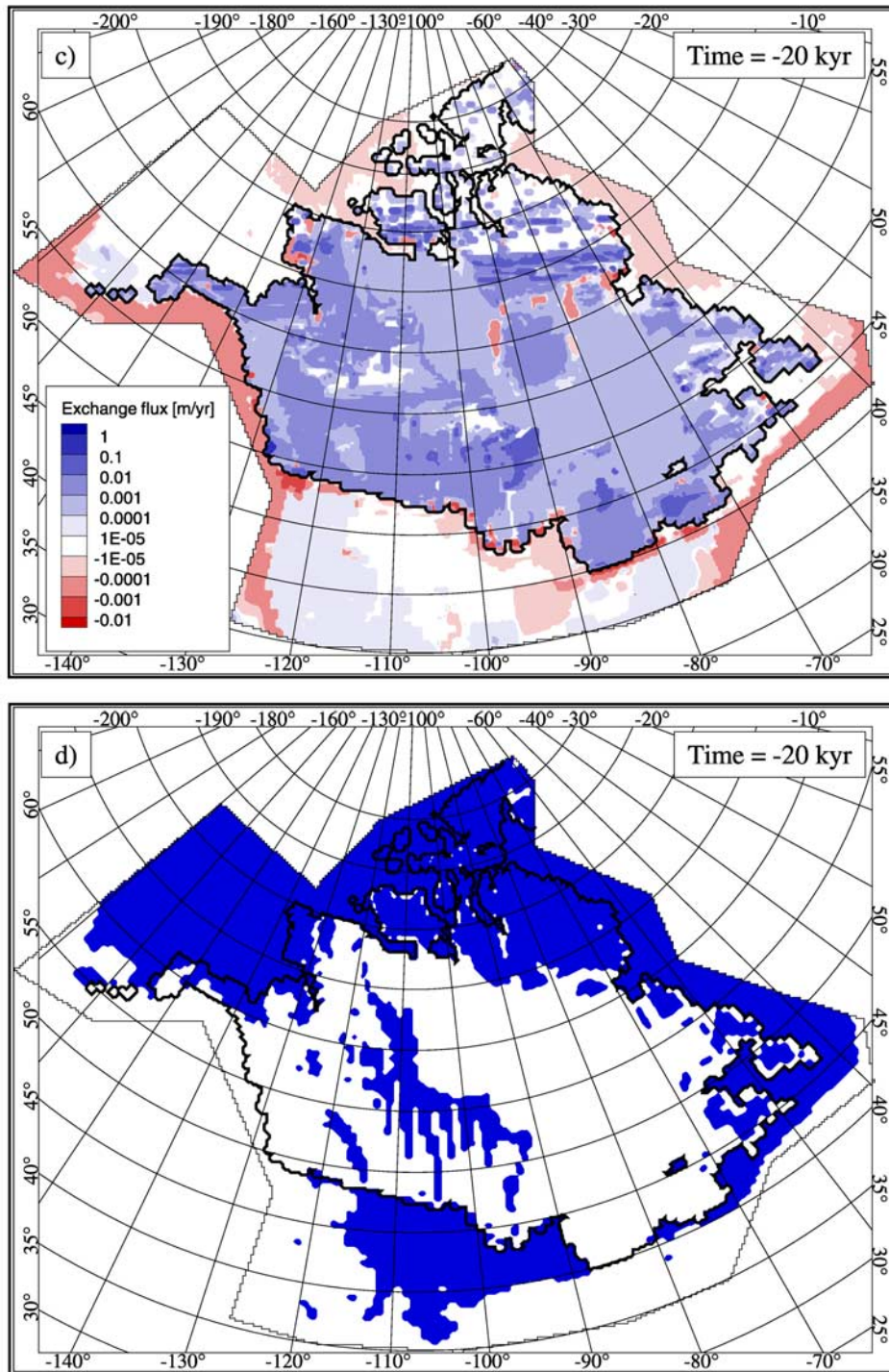
Figure 5. (continued)

[1988] gives a range between 10 and 300 mm/a. *Thorne* [2004], on the basis of a detailed water budget in three small catchments located near the Underground Research Laboratory in Manitoba, reports a recharge rate of about 2 mm/a. This is probably a more representative value for recharge into exposed Shield rocks. It will be seen that the discrepancy between our calculations and measurements may be related to a thin, more permeable, till layer over the bedrock, which favors infiltration.

6.2. Exchange Flux Sensitivity to the Loading Efficiency Parameter

[39] During the literature review, it was found that most of the studies that coupled glaciations to groundwater flow models do not account for the ice sheet loading. An ice sheet of a few kilometers thickness has a weight sufficient to depress the Earth's crust by about 1 km, and it is unlikely that it would not have an impact on subsurface pore
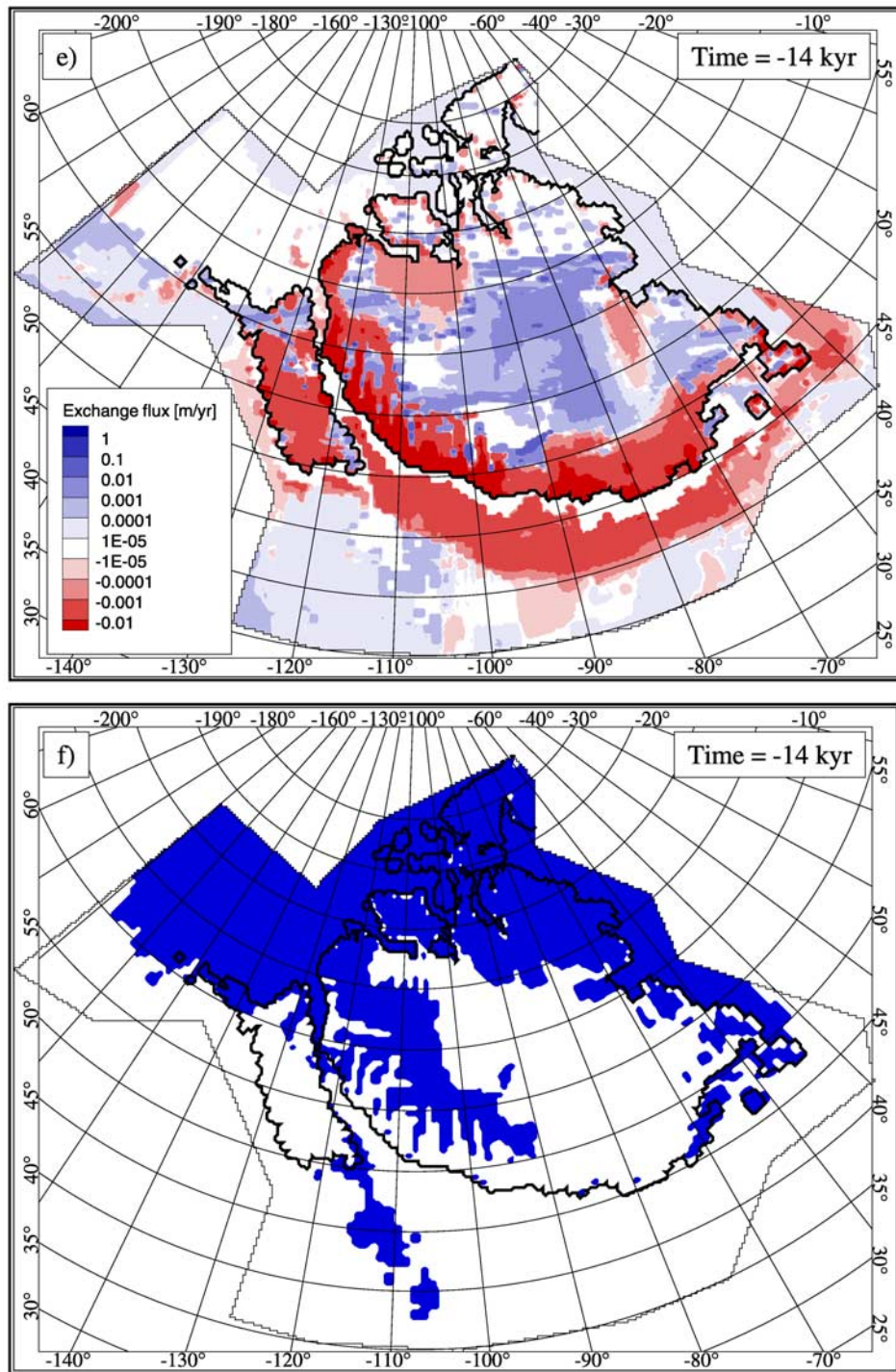
Figure 5. (continued)

pressures. Therefore the impact sensitivity of the ice sheet loading on the surface-subsurface water exchange fluxes will be demonstrated by varying the value of the loading efficiency parameter, ζ, appearing in Equation 1. For this purpose, the value used in the base case scenario was modified while the other properties and boundary conditions remained the same.

[40] Figure 9 demonstrates the effect of varying the loading efficiency parameter on the areally averaged sub-

glacial infiltration flux. The temporal change in the subglacial infiltration flux, expressed as a volumetric rate, is shown over the glacial period for loading efficiency values of 0.0, 0.2 and 1.0. It can be seen that the subglacial infiltration is maximum when the loading efficiency is zero (i.e., no loading) and it decreases when the loading efficiency increases. In other words, if all the ice weight is transferred to the fluid because of a highly compressible media (ζ is large), there is not hydraulic gradient below the
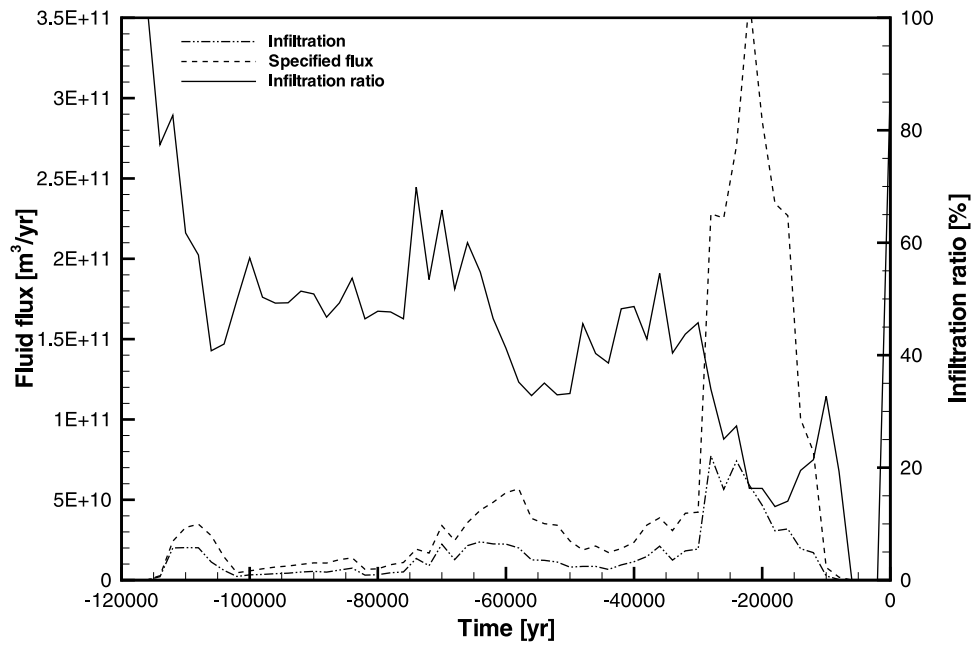
Figure 6. Total subglacial specified meltwater flux, subglacial infiltration flux, and infiltration ratio versus time throughout the last glacial cycle.

ice sheet such that no infiltration occurs. If the rock is stiff (ζ is small), the ice load is supported by the rock matrix and pore pressure does not increase in the subsurface because of ice loading. Therefore there is a strong subglacial hydraulic gradient and subglacial recharge is high.

[41] Inspecting Figure 9, it can be noted that the change in the subglacial infiltration rate is quite large for $\zeta = 1.0$ compared to that of the base case ($\zeta = 0.2$), especially during LGM when the calculated infiltration is much less with $\zeta = 1.0$. This is because the entire ice load is transferred to the subsurface fluid for $\zeta = 1.0$, thus rapidly increasing pore pressures at all depths which in turn greatly

reduces the vertical hydraulic gradient and inhibit groundwater recharge.

6.3. Permafrost Impact on Surface-Subsurface Interaction

[42] Permafrost evolution during a glacial cycle is another phenomena where large uncertainties exist regarding its distribution and timing. The role of permafrost on groundwater flow is not fully understood, although it is generally accepted that it will act as a flow barrier. In order to capture the impact of permafrost on the infiltration of subglacial meltwater, the base case simulation results are examined
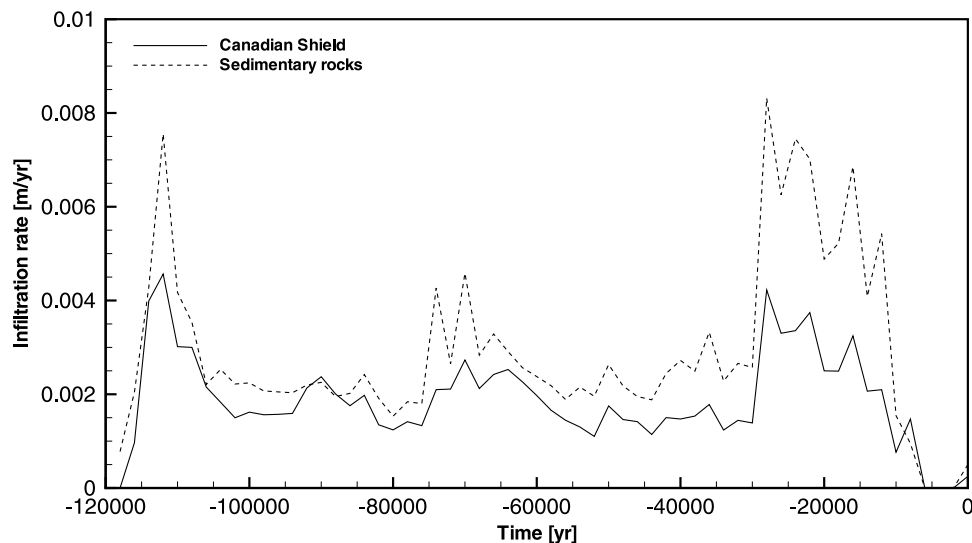

Figure 7. Mean subglacial infiltration rates for the sedimentary rocks and Canadian Shield facies.
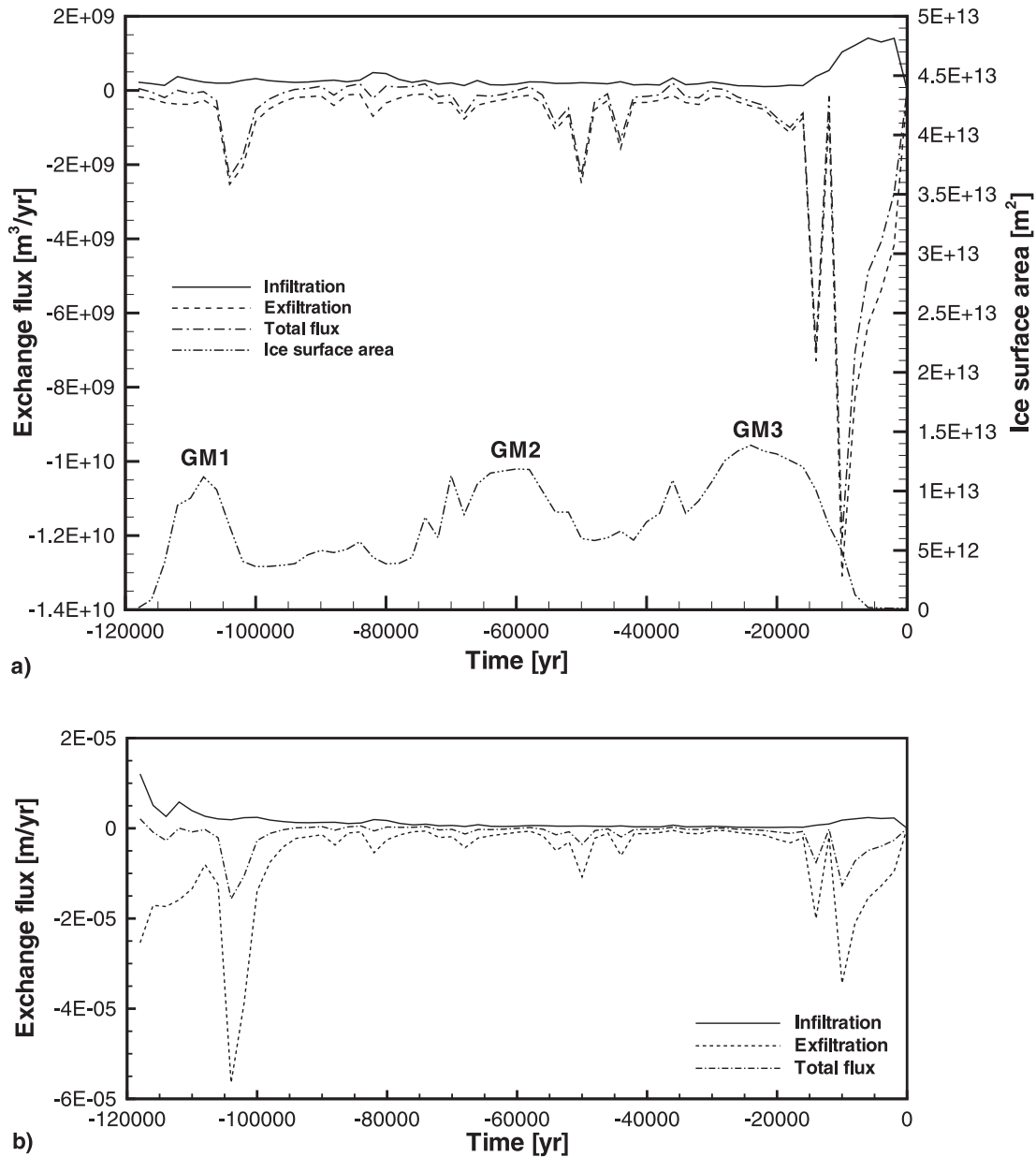
Figure 8. Periglacial exchange flux during the glacial cycle. (a) Volumetric exchange flux in m³/a. The curves represent the integration of the flux all over the periglacial environment. The ice sheet surface area is also shown with indications for glacial maximums GM1, GM2, and GM3. (b) Exchange flux in m/a; the volumetric fluxes are divided by their respective surface areas.

and will be compared to a case where the presence of permafrost is ignored.

[43] Figure 10 integrates through time the subglacial area that is covered by permafrost, the total subglacial area, as well as the subglacial area where an exchange of surface-subsurface water occurs (i.e., either meltwater infiltration or groundwater discharge). By inspection of Figure 10, it is evident that large parts of the subglacial environment are inactive in terms of surface-subsurface water interactions because the exchange flux surface area is smaller than the total subglacial surface area over the entire glacial cycle. This can be explained by examining the surficial permafrost distributions shown in Figures 5b, 5d, and 5f and comparing the patterns with those of the exchange fluxes given in

Figures 5a, 5c, and 5e. The zones where the exchange flux is low or nonexistent correspond quite well with the permafrost regions. On the other hand, some infiltration/exfiltration does occur at some permafrost locations. This becomes clear upon close inspection of the results given in Figure 10. The sum of the areas where surface-subsurface water interaction occurs and of the areas with frozen ground should match the total subglacial ice area if no water exchange flux occurs in permafrost regions; however it can be seen that the sum of the exchange flux and permafrost areas is larger than the total ice area. This indicates that some regions covered by permafrost are experiencing some infiltration or exfiltration. This can partly be explained by the presence of regions where the
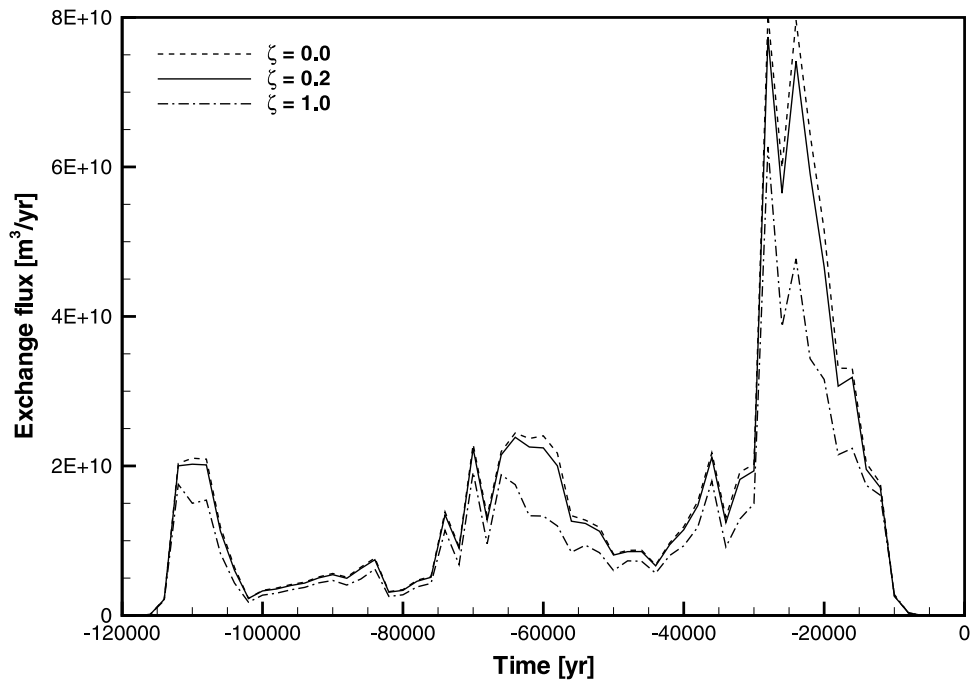
Figure 9. Subglacial infiltration flux for the base case scenario ($\zeta = 0.2$) and for cases where $\zeta = 0.0$ and $\zeta = 1.0$.

permafrost is thin enough to allow a water exchange flux despite these regions having a low hydraulic conductivity. Also, the effect of the ice loading/unloading on the surface causes the geologic materials, frozen or not, to expand and contract, which in turn forces water into or out of the porous medium (recognizing that the assumed permeability of the permafrost is nonzero, but small). Finally, it should be noted that permeabilities are linearly interpolated between their frozen and unfrozen values through each 1 ka period because the permafrost distribution is updated at this frequency, yet the flow model use 100 year time steps.

[44] Nevertheless, there are large parts of the subglacial environment that are prevented from water interaction with the subsurface because of the presence of frozen ground. Frozen materials prevent much of the surface-subsurface water interactions from occurring in both the subglacial and periglacial environments. The distribution and timing of permafrost are therefore critical to capture the impact on groundwater flow during a glaciation period.

[45] The base case scenario was therefore modified by removing the influence of permafrost formation in the model by forcing the permeabilities of the rocks to maintain
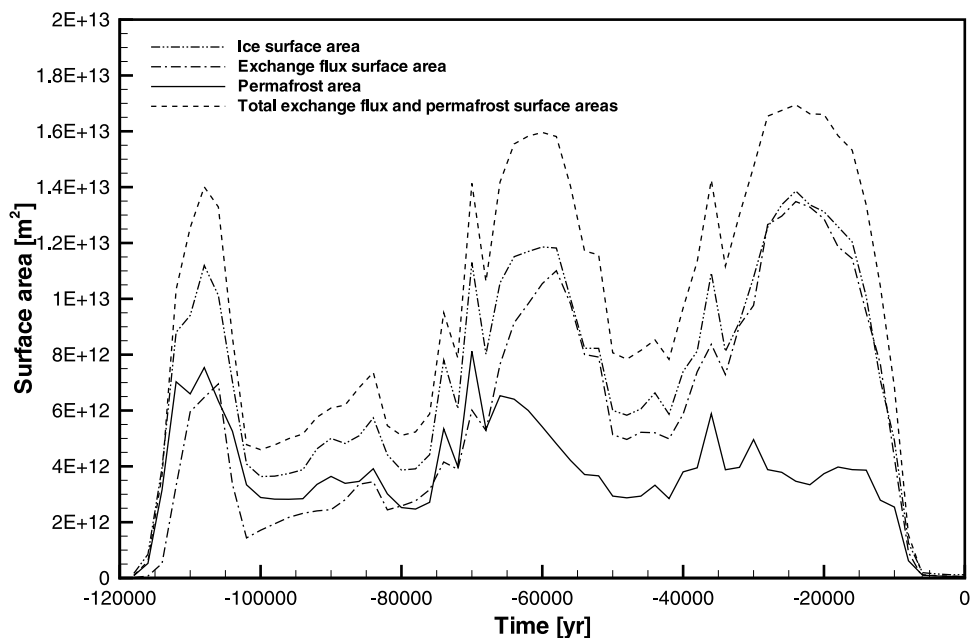

Figure 10. Ice surface, permafrost, and subglacial water exchange areas over the glacial cycle.
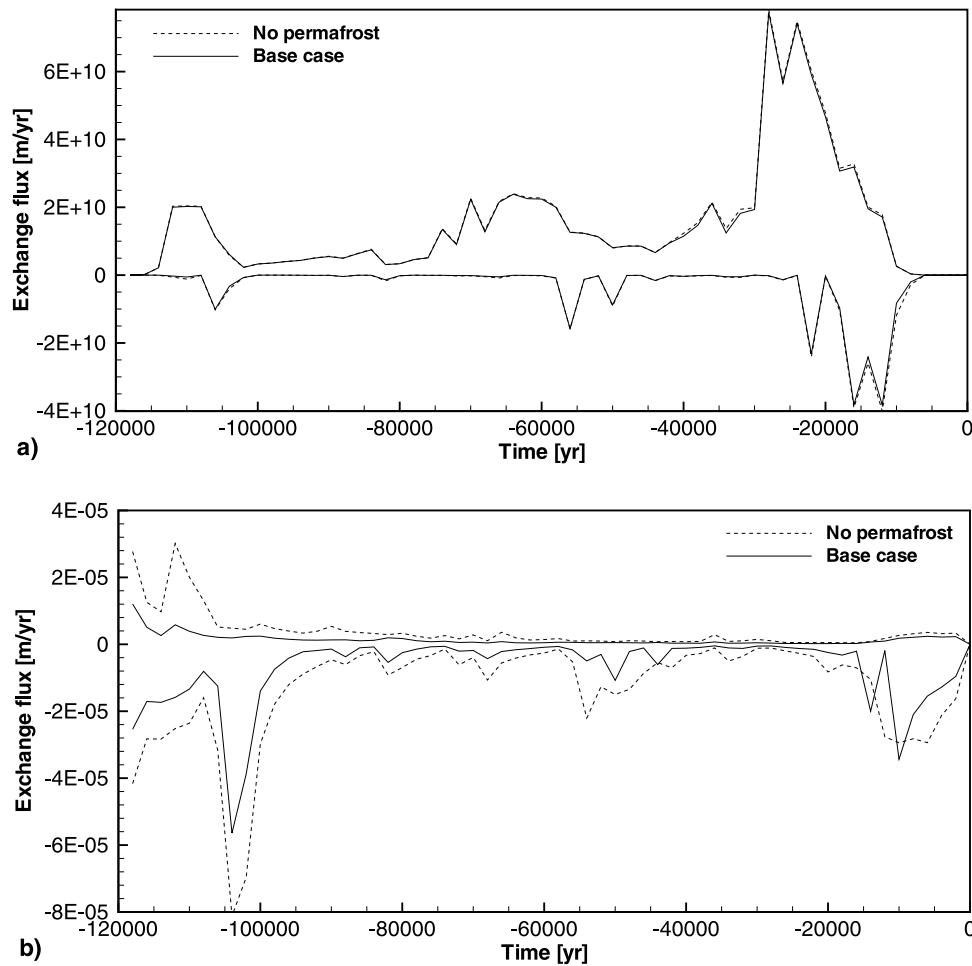
Figure 11. Infiltration (positive) and exfiltration (negative) rates for the base case scenario and the zero permafrost scenario for (a) the subglacial environment and (b) the periglacial environment.

their unfrozen values. In the subglacial environment, it appears that the neglect of permafrost does not significantly affect the computed values of the infiltration and exfiltration fluxes (Figure 11a). Subglacial meltwater is produced mainly in warm-based regions below the ice sheet where there is no permafrost and unfrozen-state permeabilities are employed. Rarely is meltwater produced in cold-based regions where permafrost exists below the ice sheet and therefore the assigned permeabilities will have little influence on the overall results in these areas because, even if the permafrost is removed, there is little or no subglacial meltwater available to infiltrate.

[46] On the other hand, the removal of the permafrost from the periglacial environment has the effect of increasing the water exchange rates between the surface and subsurface (Figure 11b). Regions that were otherwise frozen are now open for water exchange with the surface. Infiltration and exfiltration continues to occur in the unfrozen regions as it did for the base case scenario.

7. Summary

[47] The subglacial environment is a complex region in which subglacial meltwater undergoes infiltration, exfiltration and runoff. Understanding subglacial processes is highly important because they have a major impact on ice sheet dynamics, the formation of sedimentary structures and on groundwater flow and geochemical patterns. In this paper, the spatial and temporal evolution of water exchange fluxes were examined in both the subglacial and periglacial environments. The influence of permafrost was addressed, as was the sensitivity of the computed exchange fluxes to the value of the hydromechanical loading efficiency parameter.

[48] During the glacial period, the average subglacial infiltration rate into the subsurface oscillates between 0 and 6 mm/a with an average of about 2.5 mm/a, which is at least three orders of magnitudes higher than values in the periglacial environment and two orders of magnitude higher than those occurring during the interglacial period (Table 2). On average, the periglacial environment has an infiltration

Table 2. Summary of the Average Infiltration and Exfiltration Rates for the Subglacial and Periglacial Environments During the Glacial Cycle and the Last Interglacial Period

	Infiltration, m/a	Exfiltration, m/a
Subglacial environment	2.47×10^{-3}	2.03×10^{-3}
Periglacial environment	1.30×10^{-6}	7.08×10^{-6}
Interglacial period	2.87×10^{-5}	3.25×10^{-6}

rate that is much lower than the interglacial infiltration value, the later of which is about 0.03 mm/a. The calculated infiltration during the interglacial is much lower than the 2 mm/a value [*Thorne*, 2004] estimated from a hydrologic water balance of three catchments in the Canadian Shield. This difference may be due the presence of thin overburden that drain infiltrated groundwater, and that is not included in the numerical model. The ratio of the subglacial infiltration rate to the rate of subglacial meltwater production varies between 15% and 70%, with an average of 43%, which indicates that a large fraction of the meltwater actually entered the subsurface. The subglacial exfiltration rate can reach up to 12 mm/a, with an average of 2 mm/a, but occurs over a much smaller land area. This is about three orders of magnitudes higher than the amount occurring in the periglacial environment and during the interglacial period.

[49] Regarding the timing of the water exchanges, most of the subglacial meltwater infiltrates into the subsurface when the ice sheet is growing. Conversely, groundwater exfiltrates mainly during ice sheet regression. Because of the high pressures at the bed of the ice sheet, meltwater is forced downward into the subsurface during ice sheet advance and, when the ice sheet is regressing, the remnant pressure in the subsurface is higher than the basal meltwater pressure such that groundwater exfiltrates. This behavior is a consequence of the interaction between the subglacial boundary conditions and the elastic properties of the rock. A sensitivity analysis of the subglacial infiltration to the loading efficiency parameter was performed and showed that the infiltration rate into the subsurface decreases with an increase of the loading efficiency parameter such that more groundwater pressure is generated and prevents infiltration.

[50] Past analyses [*Tarasov and Peltier*, 2004] have demonstrated that geographically restricted fast flow (ice streaming) of the North American ice complex played a major role in its chronological evolution. Given that basal water pressure is a primary control for ice streaming [*Paterson*, 1994], the results of the present work suggest that infiltration/exfiltration fluxes may have a had a significant impact on the evolution of the ice sheet. Future investigations with full two-way coupling between Hydro-GeoSphere and the GSM will test this speculation.

[51] In the periglacial environment, it was shown that the flux oscillates between 0 and 0.06 mm/a, with average values in the range of 0.003 and 0.007 mm/a, respectively. This is much lower than that in the subglacial environment. Most of the exchange flux is dominated by exfiltration during ice sheet regression, as it is the case for the subglacial environment.

[52] The subglacial infiltration rate is also dependent on the rock type, as expected, because of the control exerted by rock permeability. It also appears that the difference in the subglacial infiltration rate between the different rock types increases during glacial advances.

[53] Permafrost has the effect of constraining large areas of the subglacial environment from experiencing surface-subsurface water interactions. Subglacial permafrost mainly exists below cold-based areas of the ice sheet, which are regions that do not produce subglacial meltwater. For this reason, when the presence of permafrost is ignored, little change is seen in the surface-subsurface water exchange fluxes in the subglacial environment. On the other hand, the neglect of permafrost in the periglacial environment encourages surface-subsurface water interactions and an increase of the exchange rates.

[54] Finally, pressurized groundwater below ice sheets may be an important factor to address with regard to issues such as the safe long-term disposal of radioactive wastes [*Sheppard et al.*, 1995; *Talbot*, 1999; *Heathcote and Michie*, 2004]. Since the suitability of deep geologic repositories must be demonstrated over large time scales, flow patterns under an ice sheet must be understood as they may change drastically and recharge and discharge patterns could be useful in such a task.

Appendix A: Glacial Systems Model

[55] The GSM is composed of eight components linked together and representing, respectively, surface mass balance, thermomechanically coupled ice sheet dynamics [*Tarasov and Peltier*, 1999, 2002], bed thermodynamics, basal dynamics, ice calving, isostasy, surface drainage [*Tarasov and Peltier*, 2006], and climate forcing [*Tarasov and Peltier*, 2004].

[56] The glacial systems model has been undergoing calibration for North American deglaciation against a large set of observational constraints including paleorecords of relative sea level and lake level, ice margin extent [*Dyke et al.*, 2003; *Dyke*, 2004], and present-day rates of surface uplift. The Bayesian calibration invokes Markov Chain Monte Carlo sampling of the posterior probability distribution of GSM fits to the observational constraints as predicted by a set of trained neural networks [*Tarasov and Peltier*, 2006]. The posterior probability distribution for 31 ensemble model parameters (controlling regional climate, ice calving, fast flow basal dynamics, . . .) are thereby determined by the calibration.

[57] Given the thousands of full (122 ka) glacial cycle GSM runs required for the calibration, coupling with an appropriate climate model is impossible with available computational resources. As such, the climate forcing is derived from a weighted interpolation between a present-day observational climatology [*Legates and Willmott*, 1990; *Kalnay et al.*, 1996] and a full glacial climate state (based on a composite of Paleo Model Intercomparison Project (PMIP) −21 ka General Circulation Model simulations, http://www-lsce.cea.fr/pmip/index.html). The interpolation is weighted according to a glacial index computed from a glaciological inversion of the temperature change for the summit region of Greenland [*Tarasov and Peltier*, 2003]. Twenty ensemble parameters modify the composition of the glacial climate state, regional precipitation, and the time dependence of precipitation.

[58] The bed-thermal field is computed on the basis of energy conservation. However, given the scales involved, only vertical heat conduction and latent heat effects from permafrost formation and degradation are taken into account. The deep geothermal heat flux is from the digital map of *Pollack et al.* [1993]. Surface mass balance is computed with a positive degree-day model (with temperature-dependent degree-day coefficients) and a physically based refreezing model. Surface meltwater drainage and lake storage are computed using a downslope diagnostic algorithm [*Tarasov and Peltier*, 2006]. There is also a basal

dynamics component to the model that allows till deformation and sliding when the temperature below the ice sheet is above the pressure melting point.

[59] The last component of the GSM is the isostatic adjustment process [*Peltier*, 1998]. As the ice sheet grows over the surface, its weight causes the Earth's crust to depress because of the combined viscoelastic response of the mantle and lithosphere. For an ice load of 4 km, crustal depression can exceed 1 km. This has an important impact on ice sheet dynamics, surface drainage, and temperature distributions (given the strong vertical gradient in surface air temperatures).

References

Bassin, C., G. Laske, and G. Masters (2000), The current limits of resolution for surface wave tomography in North America, *EOS Trans. AGU*, *81*(48), Fall Meet. Suppl., Abstract S12A-03.

Boulton, G. S., and G. de Marsily (1997), Hydrogeological aspects of glaciation, in *Glaciation and Hydrogeology*, *SKI Rep. 97:13*, edited by L. King-Clayton et al., pp. 33–44, Swed. Nucl. Power Insp., Stockholm.

Boulton, G. S., P. B. Caban, and K. van Gijssel (1995), Groundwater flow beneath ice sheets: Part I—Large scale patterns, *Quat. Sci. Rev.*, *14*, 545–562.

Boulton, G. S., P. B. Caban, K. van Gissel, A. Leijnse, M. Punkari, and F. H. A. van Weert (1996), The impact of glaciation on the groundwater regime of northwest Europe, *Global Planet. Change*, *12*(1–4), 397–413.

Boulton, G. S., S. Zaptsepin, and B. Maillot (2001), Analysis of groundwater flow beneath ice sheets, *SKB Tech. Rep. TR-01-06*, Swed. Nucl. Power Insp., Stockholm.

Breemer, C. H., P. U. Clark, and R. Haggerty (2002), Modeling the subglacial hydrology of the late Pleistocene Lake Michigan lobe, Laurentide Ice Sheet, *Geol. Soc. Am. Bull.*, *114*(6), 665–674.

Burt, T. P., and P. J. Williams (1976), Hydraulic conductivity in frozen soils, *Earth Surf. Processes*, *1*(4), 349–360.

Clark, I. D., M. Douglas, K. Raven, and D. Bottomley (2000), Recharge and preservation of Laurentide glacial melt water in the Canadian Shield, *Ground Water*, *38*(5), 735–742.

Dollar, P., S. K. Frape, and R. H. McNutt (1991), Geochemistry of formation waters, southwestern Ontario, Canada and southern Michigan, U.S.A.: Implications for origin and evolution, *Open File Rep. 5743*, Ont. Geol. Survey, 72 pp., Sudbury, Ont., Canada.

Douglas, M., I. D. Clark, K. Raven, and D. Bottomley (2000), Groundwater mixing dynamics at a Canadian Shield mine, *J. Hydrol.*, *235*(1–2), 88–103.

Dyke, A. S. (2004), An outline of North American deglaciation with emphasis on central and northern Canada, in *Quaternary Glaciations—Extent and Chronology*, Part II, vol. 2b, edited by J. Ehlers and P. L. Gibbard, pp. 373–424, Elsevier, New York.

Dyke, A. S., A. Moore, and L. Robertson (2003), Deglaciation of North America, *Tech. Rep. Open File 1574*, 1:7,000000 scale, Geol. Surv. of Can., Ottawa.

Ferguson, G. A. G., R. N. Betcher, and S. E. Grasby (2007), Hydrogeology of the Winnipeg formation in Manitoba, Canada, *Hydrogeol. J.*, *15*, 573–587, doi:10.1007/s10040-006-0130-4.

Flowers, G. E., and G. K. C. Clarke (2002a), A multicomponent coupled model of glacier hydrology: 1. Theory and synthetic examples, *J. Geophys. Res.*, *107*(B11), 2287, doi:10.1029/2001JB001122.

Flowers, G. E., and G. K. C. Clarke (2002b), A multicomponent coupled model of glacier hydrology: 2. Application to Trapridge Glacier, Yukon, Canada, *J. Geophys. Res.*, *107*(B11), 2288, doi:10.1029/2001JB001124.

Forsberg, C. F. (1996), Possible consequences of glacially induced groundwater flow, *Global Planet. Change*, *12*(1–4), 387–396.

Frape, S. K., and P. Fritz (1987), Geochemical trends for groundwaters from the Canadian Shield, in *Saline Water and Gases in Crystalline Rocks*, edited by P. Fritz and S. K. Frape, *Geol. Assoc. Can. Spec. Pap.*, *33*, 19–38.

Grasby, S. E., and Z. Chen (2005), Subglacial recharge into the western Canada sedimentary basin—Impact of Pleistocene glaciation on basin hydrodynamics, *Geol. Soc. Am. Bull.*, *117*(3/4), 500–514.

Grasby, S., K. Osadetz, R. Betcher, and F. Render (2000), Reversal of the regional-scale flow system of the Williston basin in response to Pleistocene glaciation, *Geology*, *28*(7), 635–638.

Heath, R. C. (1988), Hydrogeological setting of regions, in *Hydrogeology*, *Geol. N. Am.*, vol. O-2, edited by W. Back, J. S. Rosenhein, and P. R. Seaber, pp. 15–35, Geol. Soc. of Am., Boulder, Colo.

Heathcote, J. A., and U. M. Michie (2004), Estimating hydrogeological conditions over the last 120 ka: An example from the Sellafield area, UK, *J. Geol. Soc. London*, *161*, 995–1008.

Hughes, T. J. (1998), *Ice Sheets*, 343 pp., Oxford Univ. Press, Oxford, U. K.

Ingebritsen, S. E., and W. E. Sanford (1998), *Groundwater in Geologic Processes*, Cambridge Univ. Press, New York.

Jaquet, O., and P. Siegel (2003), Groundwater flow and transport modelling during a glaciation period, *SKB Tech. Rep. TR-03-04*, Swed. Nucl. Power Insp., Stockholm.

Kalnay, E., et al. (1996), The NCEP/NCAR 40-year reanalysis project, *Bull. Am. Meteorol. Soc.*, *77*, 437–471.

King-Clayton, L. M., N. A. Chapman, F. Kautsky, N.-O. Svensson, G. de Marsily, and E. Ledoux (1995), The central scenario for SITE-94: A climate change scenario, *SKB Rep. 95:42*, Swed. Nucl. Power Insp., Stockholm.

Legates, D. R., and C. J. Willmott (1990), Mean seasonal and spatial variability in gauge-corrected global precipitation, *Int. J. Climatol.*, *10*(2), 111–127.

Lemieux, J.-M. (2006), Impact of the Wisconsinian glaciation on Canadian continental groundwater flow, Ph.D. thesis, Univ. of Waterloo, Waterloo, Ont., Canada.

McEwen, T., and G. de Marsily (1991), The potential significance of premafrost to the behaviour of a deep radioactive waste repository, *SKI Rep. 91:8*, Swed. Nucl. Power Insp., Stockholm, Sweden.

McIntosh, J. C., and L. M. Walter (2005), Volumetrically significant recharge of Pleistocene glacial meltwaters into epicratonic basins: Constraints imposed by solute mass balances, *Chem. Geol.*, *222*(3–4), 292–309.

McIntosh, J. C., L. M. Walter, and A. M. Martini (2002), Pleistocene recharge to midcontinent basins: Effects on salinity structure and microbial gas generation, *Geochim. Cosmochim. Acta*, *66*(10), 1681–1700.

Neuzil, C. E. (2003), Hydromechanical coupling in geological processes, *Hydrogeol. J.*, *11*, 41–83.

Paterson, W. S. B. (1994), *The Physics of Glaciers*, 3rd ed., 480 pp., Pergamon, Oxford, U. K.

Peltier, W. R. (1998), Postglacial variations in the level of the sea: Implications for climate dynamics and solid-earth geophysics, *Rev. Geophys.*, *36*, 603–689.

Person, M., B. Dugan, J. B. Swenson, L. Urbano, C. Stott, J. Taylor, and M. Willett (2003), Pleistocene hydrogeology of the Atlantic continental shelf, New England, *Geol. Soc. Am. Bull.*, *115*(11), 1324–1343.

Person, M., J. McIntosh, V. Bense, and V. H. Remenda (2007), Pleistocene hydrology of North America: The role of ice sheets in reorganizing groundwater flow systems, *Rev. Geophys.*, *45*, RG3007, doi:10.1029/2006RG000206.

Piotrowski, J. A. (1997), Subglacial groundwater flow during the last glaciation in northwestern Germany, *Sediment. Geol.*, *111*, 217–224.

Piotrowski, J. A., and A. Kraus (1997), Response of sediment to ice sheet loading in northwestern Germany: Effective stresses and glacier bed stability, *J. Glaciol.*, *43*(145), 495–502.

Pollack, H. N., S. J. Hurter, and J. R. Johnson (1993), Heat flow from the Earth's interior: Analysis of the global data set, *Rev. Geophys.*, *31*, 267–280.

Provost, A. M., C. I. Voss, and C. E. Neuzil (1998), Glaciation and regional ground-water flow in the Fennoscandian shield; Site 94, *SKI Rep. 96:11*, Swed. Nucl. Power Insp., Stockholm.

Sheppard, M. I., B. D. Amiro, P. A. Davis, and D. R. Zach (1995), Continental glaciation and nuclear fuel waste disposal: Canada's approach and assessment of the impact on nuclide transport through the biosphere, *Ecol. Modell.*, *78*(3), 249–265.

Shoemaker, E. M. (1986), Subglacial hydrology for an ice sheet resting on a deformable aquifer, *J. Glaciol.*, *32*(110), 20–30.

Siegel, D. I. (1989), Geochemistry of the Cambrian-Ordovician aquifer system in the northern Midwest, United States, *U.S. Geol. Surv. Prof. Pap., 1405-D*.

Spencer, R. J. (1987), Origin of Ca-Cl brines in Devonian formations, western Canada sedimentary basin, *Appl. Geochem.*, *2*(2), 373–384.

Svensson, U. (1999), Subglacial groundwater flow at Äspö as governed by basal melting and ice tunnels, *SKB Tech. Rep. TR-99-38*, Swed. Nucl. Power Insp., Stockholm.

Talbot, C. J. (1999), Ice ages and nuclear waste isolation, *Eng. Geol.*, *52*(3–4), 177–192.

Tarasov, L., and W. R. Peltier (1999), Impact of thermomechanical ice sheet coupling on a model of the 100 kyr ice age cycle, *J. Geophys. Res.*, *104*(D8), 9517–9545.

Tarasov, L., and W. R. Peltier (2002), Greenland glacial history and local geodynamic consequences, *Geophys. J. Int.*, *150*, 198–229.

Tarasov, L., and W. R. Peltier (2003), Greenland glacial history, borehole constraints, and Eemian extent, *J. Geophys. Res.*, *108*(B3), 2143, doi:10.1029/2001JB001731.

Tarasov, L., and W. R. Peltier (2004), A geophysically constrained large ensemble analysis of the deglacial history of the North American ice-sheet complex, *Quat. Sci. Rev.*, *23*(3–4), 359–388.

Tarasov, L., and W. R. Peltier (2005), Arctic freshwater forcing of the Younger Dryas cold reversal, *Nature*, *435*(7042), 662–665.

Tarasov, L., and W. R. Peltier (2006), A calibrated deglacial drainage chronology for the North American continent: Evidence of an Arctic trigger for the Younger Dryas, *Quat. Sci. Rev.*, *25*(7–8), 659–688.

Teller, J. T. (1987), Proglacial lakes and the southern margin of the Laurentide Ice Sheet, in *North America and Adjacent Oceans During the Last Deglaciation*, *Geol. N. Am.*, vol. K-3, edited by W. F. Ruddiman and H. E. Wright, pp. 39–67, Geol. Soc. of Am., Boulder, Colo.

Therrien, R., R. McLaren, E. A. Sudicky, and S. Panday (2006), *HydroGeoSphere, A Three-Dimensional Numerical Model Describing Fully-Integrated Subsurface and Surface Flow and Solute Transport*, Groundwater Simul. Group, Waterloo, Ont., Canada.

Thorne, G. (2004), Hydrological processes in Precambrian Shield catchments of southeastern Manitoba, *Eos Trans. AGU*, *85*(17), Jt. Assem. Suppl., Abstract H53E-02.

van Weert, F. H. A., K. van Gijssel, A. Leijnse, and G. S. Boulton (1997), The effects of Pleistocene glaciations on the geohydrological system of northwest Europe, *J. Hydrol.*, *195*(1–4), 137–159.

Wang, H. F. (2000), *Theory of Linear Poroelasticity With Applications to Geomechanics and Hydrogeology*, 287 pp., Princeton Univ. Press, Princeton, N. J.

Wheeler, J. O., P. F. Hoffman, K. D. Cardand, A. Davidson, B. V. Sanford, A. V. Okulitch, and W. R. Roest (1997), Geological map of Canada, *Map D1860A*, Geol. Surv. of Can., Ottawa.

J.-M. Lemieux and E. A. Sudicky, Department of Earth and Environmental Sciences, University of Waterloo, Waterloo, ON, Canada N2L 3G1. (jmlemieux@alumni.uwaterloo.ca; sudicky@sciborg.uwaterloo. ca)

W. R. Peltier, Department of Physics, University of Toronto, 60 St. George Street, Toronto, ON, Canada M5S 1A7. (peltier@atmosp.physics. utoronto.ca)

L. Tarasov, Department of Physics and Physical Oceanography, Memorial University of Newfoundland, St. John's, NL, Canada A1C 5S7. (lev@physics.mun.ca)